Journal of Materials Chemistry

Cite this: J. Mater. Chem., 2012, 22, 20857

www.rsc.org/materials

COMMUNICATION

High rate performance of a $Na_3V_2(PO_4)_3$/C cathode prepared by pyro-synthesis for sodium-ion batteries

Jungwon Kang, Sora Baek, Vinod Mathew, Jihyeon Gim, Jinju Song, Hyosun Park, Eunji Chae, Alok Kumar Rai and Jaekook Kim*

Received 9th July 2012, Accepted 14th August 2012
DOI: 10.1039/c2jm34451c

A $Na_3V_2(PO_4)_3$/C cathode synthesized by a polyol-assisted pyro-synthetic reaction and subsequent sintering delivered a discharge capacity of 235 mA h g^{-1}, corresponding to an extraction of 4 Na per formula with steady capacity retention and impressive rate capabilities that maintain 56% of theoretical capacity at 2.67 C.

The long-term success of large-scale rechargeable battery systems mainly depends on two major aspects of cost and safety concerns.[1] Progressive advancement in non-aqueous electrolyte based battery technologies is visualized not only in terms of a shift from Li-ion to Na-ion battery systems but also to investigate the feasibility of developing structurally stable phosphates rather than oxides as intercalation hosts in order to suit the demands of the larger format market. Although lithium ion batteries are still being investigated for high power electric vehicle applications due to their high energy densities, the motivation for the paradigm shift to alternative technologies utilizing Na may be attributed to the low lithium reserves in the earth crust, safety issues and environmental benignity. However, sodium-ion batteries have emerged as attractive and potential energy storage systems from the standpoint of long term economic viability. The choice for phosphate-based Na-insertion hosts is obviously due to the strong covalent $(PO_4)^{3-}$ units that provide structural stability even at high charge states and address thermal safety concerns unlike commercial Li-insertion oxide hosts such as $LiCoO_2$.[2] Oxide materials may undergo oxygen evolution at high states of charge and elevated temperatures, which may lead to potentially tragic explosions.[3] Of the phosphate materials, $NaVPO_4F$,[4] $NaMPO_4$,[5,6] $Na_{1.5}VOPO_4F_{0.5}$,[7] Na_2FePO_4F,[8,9] and $NaTi_2(PO_4)_3$ (ref. 10) have been screened as active materials for sodium ion batteries.

NASICON-type $Na_3V_2(PO_4)_3$ has recently been investigated as a prospective cathode material for sodium ion batteries. The electrochemical response of the NASICON-type electrode displays two potential plateaus located at 3.4 V and 1.6 V *vs.* Na/Na^+ related to the V^{3+}/V^{4+} and V^{2+}/V^{3+} redox couple, respectively, and the theoretical capacity of this material varies between 118 and 236 mA h g^{-1} depending on the cycling potential and the variation between V^{3+}/V^{4+} and V^{2+}/V^{3+} redox states. The low potential plateau exhibited by this material makes it versatile to be used as an anode in rechargeable alkali battery systems.[11] The realization of 100% theoretical capacities in this NASCION-type material is difficult owing to the poor electronic conductivity of phosphates. The strategies adopted to overcome this scarcity are mainly focused on providing electrically conductive coatings on particle surfaces[12] and/or reducing particle sizes.[13] To date, few reports on $Na_3V_2(PO_4)_3$ prepared by solid-state reactions are available and the electrochemical performances of this NASICON-type electrode demonstrate capacity limitations at high charge–discharge rates.[11,14] The limited rate performance may be attributed to the inevitable particle growth due to prolonged sintering ($T \geq 24$ h) at elevated temperatures ($T \geq 800$ °C). The studies also suggested that significant electrode performance is feasible by optimizing particle-sizes.

Herein, we adopt a polyol mediated pyro-synthetic method, wherein the polyol medium acts as the solvent and the conductive carbon source, to synthesize amorphous carbon-coated $Na_3V_2(PO_4)_3$ particles. The as-prepared sample was sintered for time durations ($T \leq 5$ h) at elevated temperatures to produce nanoparticles with highly crystalline characteristics. Although the short sintering time periods employed are not sufficient to trigger particle growth, the high sintering temperatures unavoidably facilitate slight particle growth through aggregation but not to a large extent. Conventional strategies to produce $Na_3V_2(PO_4)_3$ particles require prolonged heating under high temperatures wherein detrimental particle growth is inevitable and micro-sized particles result unlike in the present case where the carbon formed from the polyol combustion and the short sintering time durations tend to limit particle growth even at high temperatures. Hence a major nano-sized domain appears to exist in addition to agglomerated micro-sized particles. A dual-porosity feature is also existent in this cathode. Moreover, the painting of a thin carbon layer on the particle surface tends to prevent particle growth at high temperatures and appears to permit decent electronic conductivity. Further, the feasibility of forming a conductive network may also improve particle connectivity. The resulting carbon-coated $Na_3V_2(PO_4)_3$ nanoparticles (hereafter denoted as NVP/C) exhibit significantly improved electrochemical performances in a Na-ion cell even at high charge–discharge rates.

$Na_3V_2(PO_4)_3$ powders were obtained by a pyro-synthetic approach of combustion using sodium acetate ($C_2H_3NaO_2$, ≥99% – ALDRICH), vanadium acetyl-acetonate ($C_{15}H_{21}O_6V$, 97% – ALDRICH), and phosphoric acid (H_3PO_4, ≥85% – DAEJUNG).

Department of Materials Science and Engineering, Chonnam National University (WCU), Gwangju 500-757, Korea. E-mail: jaekook@chonnam.ac.kr; Fax: +82-62-530-1699; Tel: +82-62-530-1703

The starting precursors were dissolved in 80 mL of tetraethylene glycol ($C_8H_{18}O_5$, 99.5% – DAEJUNG) in the molar ratio 1.5 : 1 : 1.5 (Na : V : P) and stirred for 24 hours at room temperature. After subsequently obtaining a homogenous solution, 50 ml of inflammable liquid thinner was added to the solution which was then stirred for 30 min. The final solution was uniformly poured onto a hot-plate maintained at 470 °C. The flammable solution was ignited with a torch to induce a self-extinguishable combustion process. Subsequently, the as-prepared powder was annealed at 800 °C for 5 h ($T \leq$ 5 h) under argon atmosphere to obtain the carbon-coated network – $Na_3V_2(PO_4)_3$ with high crystallinity.

Powder X-ray diffraction data of the obtained samples were recorded using a Shimadzu X-ray diffractometer with Ni-filtered Cu Kα radiation (λ = 1.5406 Å) operating at 40 kV and 30 mA within the scanning angle, 2θ, range of 10–80° in steps of 0.01°. The particle morphologies and sizes were determined by field emission-scanning electron microscopy (FE-SEM) using an S-4700 model from HITACHI. The high-resolution transmission electron microscopy (HR-TEM) and transmission electron microscopy (TEM) images were recorded using an FEI Tecnai F20 at a 200 kV accelerating voltage.

The electrochemical properties of the $Na_3V_2(PO_4)_3$ particles were evaluated using sodium metal as the reference electrode. The cathode was fabricated by mixing the active material with 30 wt% carbon black and polytetrafluoroethylene was used as a binder. The presence of 16 wt% carbon content in the sample was taken into account while mixing the active materials with conductive carbon. This mixture was pressed onto a stainless steel mesh and dried under vacuum at 150 °C for 10 h. The cell consisted of a cathode and a sodium metal anode separated by glass fiber. The electrolyte used was a propylene carbonate (PC) containing 1 M $NaClO_4$.

X-ray diffraction (XRD) patterns of the samples synthesized by pyro-synthesis are shown in Fig. 1. The as-prepared sample shows amorphous characteristics whereas all the diffraction lines in the annealed sample were indexed to a pure NASICON-type $Na_3V_2(PO_4)_3$ structure without any unwanted impurities similar to previous reports.[11,14–16]

Fig. 2a shows the low-magnification FE-SEM image of NVP/C that appears to reveal a few micro-sized particles (2–5 μm) dispersed at random locations in addition to apparently smaller sized particles.

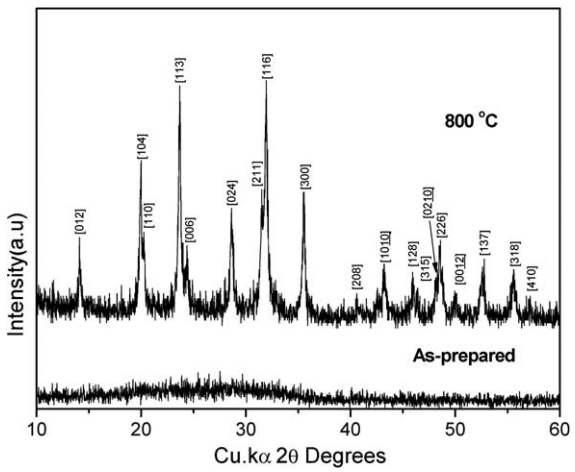

Fig. 1 X-ray diffraction patterns for the as-prepared and sintered samples obtained by the polyol-assisted pyro-synthetic reaction.

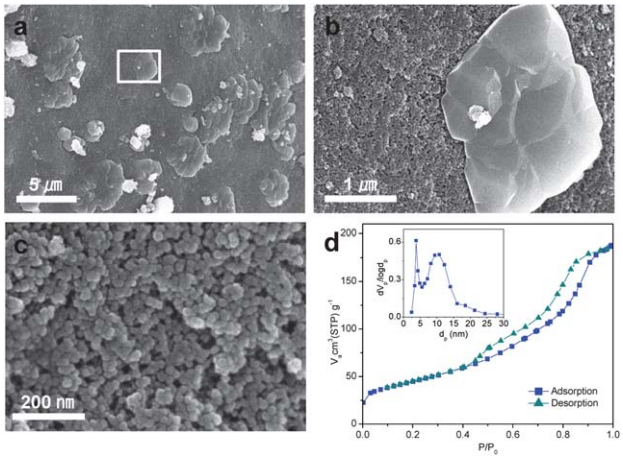

Fig. 2 SEM images of NVP prepared by pyro-synthetic reaction under (a and b) low magnification and (c) high magnification. (d) The N_2 adsorption–desorption isotherm and (inset) the pore-distribution plots for the NVP synthesized by pyro-synthetic reaction.

The magnified image of the location (earmarked in Fig. 2a) at proximity to the region of the micro-sized particles, shown in Fig. 2b, reveals smaller particles of sizes in the nano-scale range near an aggregated micro-sized particle. It appears seemingly possible that the agglomerated micro-particles are formed due to sintering of the as-prepared sample at elevated temperatures.[11] Nevertheless, a major portion of the low magnification image in Fig. 2a reveals the presence of nanoparticles in the sample annealed at high temperatures (800 °C). It is probable that the short sintering time ($T \leq$ 5 h) eliminates the possibility of extensive particle growth since the as-prepared powder obtained after polyol combustion is loosely bound at the atomic level and permits nanoparticle formation with highly crystalline nature during sintering. Similar properties were observed for the sample sintered for 1 h and the detailed thermal studies will be published elsewhere. Furthermore, the homogeneously drenched carbon sources from the organic solvent (polyol) also prevent particle growth while providing a reducing atmosphere and maintaining V(III) oxidation states. The SEM image in Fig. 2c indicates that the average diameters of the nano-scale particle range between 20 and 30 nm and the nanoparticles appear to arrange themselves in such a way to form porous morphologies. In order to elucidate further on the sample porous morphologies, the N_2 adsorption–desorption was obtained for the NVP/C and the results, presented in Fig. 2d, reveal a type-IV isotherm plot with an H1 hysteresis loop at relative pressure (p/p_0) ~0.4 to 0.9. The Barrett–Joyner–Halenda (BJH) pore-size distribution plot (Fig. 2d, inset) reflects that pores of two different sizes are formed.

The smaller sized pore has a narrow distribution at 3.77 nm with an average pore volume of 0.28 cm^3g^{-1} and the other pore-size has a broad distribution around 10 nm. The pore-sizes that are estimated to be in the mesopore ranges may influence the intercalation behavior and hence the electrochemical storage process in Li-ion battery electrodes.[17,18] A sample surface area of 159.4 m^2g^{-1} was determined by the Bruner–Emmett–Teller (BET) technique and the high value probably results from the contribution of the nanoparticles in the sample. Since the as-prepared sample was sintered in the argon atmosphere, carbon residues formed may also contribute to the surface area. The porosity studies clearly indicate that the

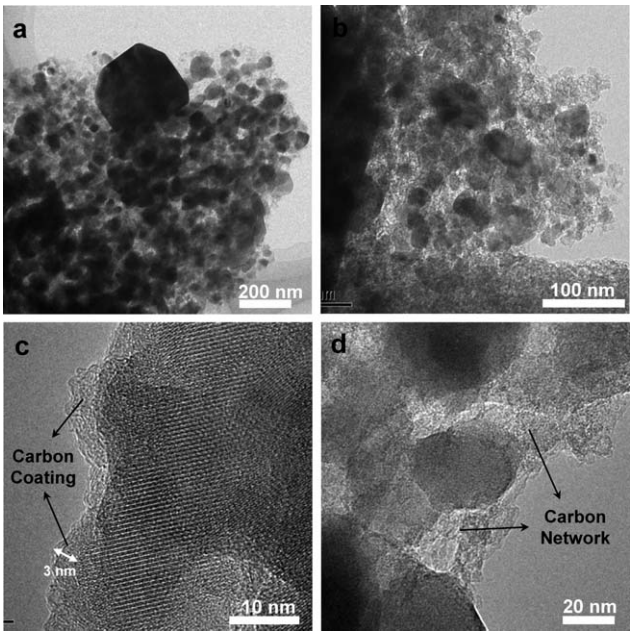

Fig. 3 (a and b) TEM images of the NVP/C synthesized by pyro-synthetic reaction and (c and d) high-resolution TEM images of NVP/C.

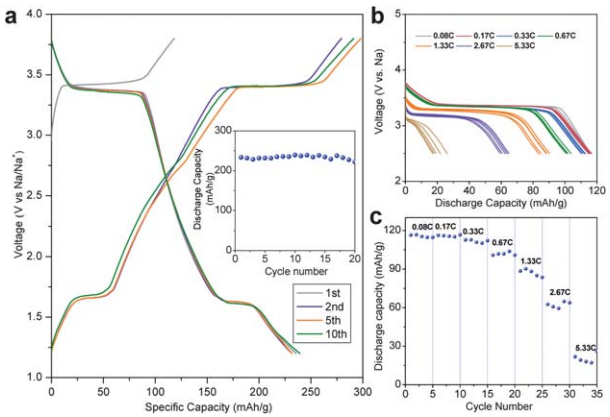

Fig. 4 (a) The electrochemical profiles of NVP/C displayed within the voltage range 3.8–1.5 V at a current density of 0.08 C-rate. The inset shows the cycle performance. (b) The voltage profiles and (c) the discharge capacities obtained at various C-rates for the NVP/C electrode *versus* Na.

nanoparticles possibly arrange themselves to form inter-particle voids that are analogous to structures with mesoporous morphologies.[19,20] The continuous network of pore-like cavities promotes facile permeation of ionic moieties in the electrolyte and facilitates improved electrical conductivities compared to those afforded by dispersed nanoparticles.[21] To glean information on the carbon distribution in the sample, TEM images of the NVP/C were recorded and the results are shown in Fig. 3. An almost uniform distribution of nano-sized particles is observed except for a few bigger sized particles of diameters of a few hundred nanometers, as revealed in Fig. 3a and b, which may be attributed to the unavoidable particle growth occurring at high sintering temperatures. The high resolution image in Fig. 3c reveals a carbon painted layer of thickness ~2 to 5 nm on the particle boundaries of the present sample. Further, Fig. 3d appears to indicate a carbon network formed between the particles since the color contrast of the carbon in Fig. 3c matches well with the network-type attachments between particles in Fig. 3d. The carbon content estimated by the elemental analysis is 16.45% and it appears to be sufficient for the carbon layer and network formation. It is anticipated that the combined factors of dual porosity, high sample surface area, surface carbon painting and the presence of carbon-networks within the sample will contribute to the electrode performance of NVP/C in sodium batteries.

Fig. 4a presents the initial charge and subsequent discharge–charge curves of NVP/C in the voltage range of 3.8–1.2 V at a current density of 10 mA g^{-1}. The delivered initial specific charge and discharge capacities are 117 and 235 mA h g^{-1}, which correspond to an extraction of 2 Na and an insertion of 4 Na per formula, respectively, and an average discharge capacity of 234 mA h g^{-1} is maintained thereafter on extended cycling. The registered specific capacities are well consistent with 100% theoretical charge and discharge capacities of 117 and 234 mA h g^{-1}. To our knowledge, the present values are the best reported among NASICON-$Na_3V_2(PO_4)_3$ cathodes available in the literature. The electrochemical curves display two distinct plateaus at 3.4 and 1.62 V which may correspond to the characteristic V^{4+}/V^{3+} ($Na_{1+x}V_2(PO_4)_3$, $x \leq 2$) and V^{3+}/V^{2+} ($Na_{3+x}V_2(PO_4)_3$, $x \leq 2$) redox couples, respectively.[14] Further, the curves reveal that 4 Na per formula is reversibly intercalated and the performance is competitive as in large scaled sodium storage systems. The cycle performance of the NVP/C electrode displayed in the inset of Fig. 4a reveals that steady capacities are maintained until 20 cycles.

Fig. 4b shows the C-rate performance of the NVP/C electrode in the voltage range of 3.8–2.5 V to test its compatibility as a 3.4 V cathode *vs.* Na/Na^+. A discharge capacity in the proximity of 117 mA h g^{-1} (theoretical capacity) corresponding to 2 Na per formula is realized at low rates of 0.08, 0.17, and 0.33 C. At 1.33 C rate, a discharge capacity of 88 mA h g^{-1} corresponding to 75% of theoretical value is maintained. A remarkable average capacity of about 65 mA h g^{-1}, corresponding to 56% of theoretical capacity, is achieved at rates as high as 2.67 C. The capacity enhancement and the impressive rate capabilities in the prepared NASICON cathode may be explained on the basis of the polyol medium that facilitates sufficient carbon painting on the nanoparticle surfaces that can act as electrical conduits during electrochemical reaction. The carbon-network appears to favor better particle-connectivity and hence improve the electronic conductivities and contribute to rate performance. Although the presence of micro-particles in the sample is detrimental to electrode performance, a major portion of nano-scale particles that tend to arrange themselves in such a way to form pore morphologies appear to be significant. Moreover, the dual porosity and high surface area can contribute to enhanced electrode/electrolyte contact areas and promote greater ion-diffusion during electrochemical reaction. Further, the dual porosity feature was identified to correlate with high rate performances in Li-ion battery electrodes.[18] The promising electrode performance is not only comparable to that of known NASICON-$Na_3V_2(PO_4)_3$ cathodes but also comparable to other cathode materials for Na ion batteries with respect to power densities.[22–24] The achievement of electrodes with porous morphologies of narrow pore-size distributions without the use of any expensive templates/structure directing agents during synthesis remains highly significant.

Furthermore, the present synthetic strategy offers a reliable and efficient approach to obtain useful nanomaterials since the exothermic energy released by the polyol combustion is well utilized for the nucleation and crystallization of nanoparticles and this aspect tends to maintain the energy consumption during synthesis at a minimum except for the post-heat treatment. Also, the reaction time for the pyro-synthesis is completed in a few seconds and evades the time-consuming filtration–separation techniques followed for wet-syntheses.

In summary, we report on a carbon-coated highly crystalline $Na_3V_2(PO_4)_3$ electrode with a conductive carbon-network among the mostly nano-scaled particles. Our NVP/C electrode shows remarkable storage abilities among the NASICON samples studied so far. The voltage curves clearly depict the characteristic potential of higher and lower plateaus at 3.4 and 1.62 V corresponding to V^{4+}/V^{3+} and V^{3+}/V^{2+} redox couples, respectively. An average discharge capacity of 234 mA h g^{-1} is reversibly achieved at a current density of 10 mA g^{-1} during extended cycles. When employed as a 3.4 V cathode *versus* Na which is analogous to $LiFePO_4$ in a Li cell, the synthesized NVP/C electrode exhibited an average discharge capacity of 117 mA h g^{-1} corresponding to 100% theoretical values at low rates of 0.08, 0.17, and 0.33 C. At high rates of 2.67 C, a remarkable discharge capacity of about 65 mA h g^{-1} is achieved. The outstanding electrochemical performance of NVP/C may be attributed to the combined contributions of carbon painting, carbon networking, dual porosity, and high sample surface areas. The present synthetic strategy thus offers the possibilities to achieve high rate capability even in an electronically unfavorable phosphate electrode for rechargeable sodium ion batteries given that the comparatively larger ionic radius of the Na ion (1.02 Å) than that of the Li ion (0.76 Å) tends to hinder smooth intercalation into the Na-electrode hosts.

Acknowledgements

This research was supported by WCU (World Class University) program through the Korea Science and Engineering Foundation funded by the Ministry of Education, Science and Technology (R32-20074).

Notes and references

1 M. Armand and J. M. Tarascon, *Nature*, 2008, **451**, 652–657.
2 T. Nagaura and K. Tozawa, *Prog. Batteries Sol. Cells*, 1990, **9**, 209–217.
3 J. Jiang and J. Dahn, *Electrochem. Commun.*, 2004, **6**, 39–43.
4 J. Barker, M. Y. Saidi and J. L. Swoyer, *Electrochem. Solid-State Lett.*, 2003, **6**, A1–A4.
5 K. Zaghib, J. Trottier, P. Hovington, F. Brochu, A. Guerfi, A. Mauger and C. M. Julien, *J. Power Sources*, 2011, **196**, 9612–9617.
6 K. T. Lee, T. N. Ramesh, F. Nan, G. Botton and L. F. Nazar, *Chem. Mater.*, 2011, **23**, 3593–3600.
7 F. Sauvage, E. Quarez, J.-M. Tarascon and E. Baudrin, *Solid State Sci.*, 2006, **8**, 1215–1221.
8 Y. Kawabe, N. Yabuuchi, M. Kajiyama, N. Fukuhara, T. Inamasu, R. Okuyama, I. Nakai and S. Komaba, *Electrochem. Commun.*, 2011, **13**, 1225–1228.
9 N. Recham, J.-N. Chotard, L. Dupont, K. Djellab, M. Armand and J.-M. Tarascon, *J. Electrochem. Soc.*, 2009, **156**, A993–A999.
10 S. I. Park, I. Gocheva, S. Okada and J.-I. Yamaki, *J. Electrochem. Soc.*, 2011, **158**, A1067–A1070.
11 L. S. Plashnitsa, E. Kobayashi, Y. Noguchi, S. Okada and J.-I. Yamaki, *J. Electrochem. Soc.*, 2010, **157**, A536–A543.
12 E. M. Bauer, C. Bellitto, M. Pasquali, P. P. Prosini and G. Righini, *Electrochem. Solid-State Lett.*, 2004, **7**, A85–A87.
13 D. H. Kim and J. Kim, *Electrochem. Solid-State Lett.*, 2006, **9**, A439–A442.
14 Z. Jian, L. Zhao, H. Pan, Y.-S. Hu, H. Li, W. Chen and L. Chen, *Electrochem. Commun.*, 2012, **14**, 86–89.
15 J. Gaubicher, C. Wurm, G. Goward, C. Masquelier and L. Nazar, *Chem. Mater.*, 2000, **12**, 3240–3243.
16 B. L. Cushing and J. B. Goodenough, *J. Solid State Chem.*, 2001, **162**, 176–181.
17 Y. Ren, A. R. Armstrong, F. Jiao and P. G. Bruce, *J. Am. Chem. Soc.*, 2010, **132**, 996–1004.
18 N. N. Sinha, C. Shivakumara and N. Munichandraiah, *ACS Appl. Mater. Interfaces*, 2010, **2**, 2031–2038.
19 K. Kaneko, *J. Membr. Sci.*, 1994, **96**, 59–89.
20 K. Kandori, T. Kuwae and T. Ishikawa, *J. Colloid Interface Sci.*, 2006, **300**, 225–231.
21 B. T. Holland, C. F. Blanford, T. Do and A. Stein, *Chem. Mater.*, 1999, **11**, 795–805.
22 S.-W. Kim, D.-H. Seo, X. Ma, G. Ceder and K. Kang, *Adv. Energy Mater.*, 2012, **2**, 710–721.
23 M. D. Slater, D. Kim, E. Lee and C. S. Johnson, *Adv. Funct. Mater.*, 2012, DOI: 10.1002/adfm.201200691.
24 V. Palomares, P. Serras, I. Villaluenga, K. B. Hueso, J. C. González and T. Rojo, *Energy Environ. Sci.*, 2012, **5**, 5884–5901.

